Materials Transactions, JIM, Vol. 38, No. 4 (1997), pp. 277 to 284

Phase Transformation and Crystal Structures of Ti_2Ni_3 Precipitates in Ti-Ni Alloys

Toru Hara*, Takuya Ohba*, Kazuhiro Otsuka**
and Minoru Nishida***

*Department of Materials Science and Engineering, Teikyo University, Utsunomiya, Tochigi 320, Japan
**Institute of Materials Science, University of Tsukuba, Tsukuba, Ibaraki 305, Japan
***Department of Materials Science and Engineering, Faculty of Engineering, Kumamoto University, Kurokami, Kumamoto 860, Japan

In Ni-rich Ti-Ni alloys, three kinds of precipitates such as $TiNi_3$, Ti_2Ni_3 and Ti_3Ni_4 appear with aging heat-treatments. The shape memory effect and superelasticity of the alloys are greatly affected by the presence of these precipitates. It is interesting to note that the Ti_2Ni_3 precipitate itself exhibits a phase transformation. However, the characteristics of this transformation is not understood in detail as yet. In the present study, the characteristics of this transformation were studied from crystallographic point of view. The crystal structures of the low- and the high-temperature phases were determined by combining several techniques such as electron diffraction, convergent beam electron diffraction, high resolution electron microscopy and powder X-ray diffraction with the Rietveld analysis. The results of these analyses revealed that the space group of the low- and the high-temperature phases are *Bbmm* and *I4/mmm*, respectively. It was reported that the $Ti_2(Ni, Cu)_3$ alloy shows a similar transformation. The relevance of the transformation in this alloy to Ti_2Ni_3 precipitates is also discussed.

(Received October 7, 1996)

Keywords: *crystal structure, TiNi alloy, Ti_2Ni_3 precipitate, martensitic transformation, transmission electron microscopy, convergent beam electron diffraction, high resolution electron microscopy, X-ray diffraction, the Rietveld method*

I. Introduction

In Ni-rich Ti-Ni shape memory alloys, three kinds of precipitates, Ti_2Ni_3, Ti_3Ni_4 and $TiNi_3$, appear by appropriate aging heat-treatments. Nishida *et al.* studied the precipitation processes and reported the TTT (time-temperature-transformation) diagrams for several compositions of alloys[1].

Nishida and Wayman[2] found that the Ti_2Ni_3 precipitate exhibits a phase transformation. They studied the transformation behavior by using a transmission electron microscope (TEM) with a heating specimen holder and reported as follows.

(i) The precipitate shows two step transformations; that is, it transforms from the tetragonal high-temperature phase to the monoclinic low-temperature phase via the orthorhombic intermediate phase with cooling.

(ii) There are differences of the morphologies among these phases. An antiphase-like contrast is observed in the intermediate orthorhombic phase and the needle-like domain contrast is observed in the monoclinic phase. Needle-like domain contrast is caused by twins whose index of the twin boundary is $\{120\}_L$†.

† In this paper, the suffixes of the index indicate as follows: H: High temperature phase, L: Low temperature phase. When it is needed to distinguish between matrix and twin, the following notation will be used. M: Matrix of the low-temperature phase, T: Twin of the low-temperature phase.

Concerning the crystal structure of these three phases in Ti_2Ni_3 precipitate, there is no information, except for the lattice parameters. According to Nishida and Wayman[2], diffraction patterns for the tetragonal high-temperature phase were indexed by using the lattice parameters of ternary Cu added $Ti_2(Ni, Cu)_3$ reported by Van Loo *et al.*[3] Since the electron diffraction patterns of $Ti_2(Ni, Cu)_3$ and those of the Ti_2Ni_3 are quite similar, the crystal structure of $Ti_2(Ni, Cu)_3$ can be considered to be the same as that of Ti_2Ni_3 and the phase transformation was expected. Nishida *et al.*[4] made a single phase specimen with the composition of Ti-56.5 at.%Ni-3.5 at.% Cu and determined the lattice parameters with the X-ray diffraction experiments. The series of their study showed that the structures and morphologies of $Ti_2(Ni, Cu)_3$ and the characteristic of the transformation are quite similar to those of Ti_2Ni_3.

The purpose of the present study is to determine the crystal structure of the Ti_2Ni_3 precipitate and clarify the characteristics of the transformation in the Ti_2Ni_3 precipitate from the crystallographic point of view. The similarity between Ti_2Ni_3 and $Ti_2(Ni, Cu)_3$ is also discussed.

II. Experimental Procedure

1. Sample preparation

An X-ray diffractometer, and optical and transmission

electron microscopes were used for the experiments. The following two kinds of samples were prepared for each experiment:

(1) Ti_2Ni_3

Button shaped ingots, whose composition is 48.0 at.% Ti–52.0 at.%Ni, were made by Ar arc melting with a purity of 99.5%Ti and 99.97%Ni. Specimens were sealed in evacuated quartz capsules. Heat-treatment condition was 1273 K for 3.6 ks as a solution treatment, followed by water quench without breaking the capsule. Several kinds of aging treatments were applied to make Ti_2Ni_3 precipitates with varying the aging time at 973 K, and the specimens were ice water quenched after the aging. Aging conditions by Nishida and Wayman[2] were followed. The results of optical microscopy observation revealed that the amount of the precipitates increases with the aging time until 180 ks and then decreases with longer aging time. This phenomenon is understood such that Ti_2Ni_3 precipitates are replaced by $TiNi_3$ precipitates for longer time aging[1]. Aging times of 36, 90, 180 ks were chosen for the following electron microscope observation and X-ray diffraction experiment.

(2) $Ti_2(Ni, Cu)_3$

According to Nishida and Wayman[2], a small addition of Cu stabilizes the single phase of $Ti_2(Ni, Cu)_3$ which has the same crystal structure of Ti_2Ni_3. Composition of 40.0 at.%Ti–56.5 at.%Ni–3.5 at.%Cu was chosen to make a single phase of $Ti_2(Ni, Cu)_3$. Ingots were made by Ar arc melting. Specimens were sealed in an evacuated quartz tube. Heat-treatment conditions were as follows: 1273 K for 3.6 ks as a solution treatment followed by ice water quench without breaking a capsule, and then aged at 1073 K for 360 ks to make a single phase, which is followed by ice water quench again. The $Ti_2(Ni, Cu)_3$ was a single phase as far as we observed.

2. Electron microscopy experiment

Specimens for the electron microscope observations were prepared by using the twin jet electro-polishing apparatus STRUERS TENUPOL 3 with the solution of H_2SO_4(20 vol.%) + CH_3OH(80 vol.%) at 20 V, 0.25 A at 283 K. Conventional electron microscope observation, electron diffraction and convergent beam electron diffraction (CBED) were carried out using the JEOL JEM-2000FX2 at the accelerating voltage of 200 or 120 kV with a double tilt specimen holder. For the high resolution electron microscope observations (HREM), JEOL JEM-2010 was used. Multislice calculation program, MacTempas, was used for the analysis of the lattice image.

3. X-ray diffractometer measurements

The diffractometer used in this experiments was Shimadzu XD-610 with a graphite analyzer and Cu radiation. Slit systems, scattering slit (SS), divergence slit (DS) and receiving slit (RS), were 1 deg., 1 deg. and 0.3 mm, respectively. Data collections were done by the step scan mode with intervals of 0.02 degree and 4 s for each step. Operation conditions were at 40 kV, 30 mA, and measured 2θ range was from 30 to 100°. A specimen heating holder was used for the measurements. The measurements were carried out at various temperatures between 298 and 373 K at every 5 K on heating and cooling.

The Pawley method, which is a kind of the whole powder pattern decomposition method, was applied to determine the lattice parameters and various fitting parameters such as the profile function. For the refinements of the structure parameters, the Rietveld method was used. The final fitting parameters and lattice parameters refined by the Pawley method were used for the initial value for the Rietveld method. The computer programs used in this analysis were WPPD[5] for the Pawley method, and RIETAN[6] for the Rietveld method. The initial structure models for the Rietveld refinements are described in the next section.

III. Results and Discussions

1. Electron microscope observations

Electron microscopy observations and electron diffraction experiments were carried out at room temperature for the following two purposes. First is to clarify the difference between Ti_2Ni_3 and $Ti_2(Ni, Cu)_3$. Second is to determine the space group of the low-temperature phase of Ti_2Ni_3 and $Ti_2(Ni, Cu)_3$. For the first purpose, the morphology and the intensity distribution of electron diffraction patterns for these two phases are compared. Figure 1 shows a typical morphology of the Ti_2Ni_3. Twin-related needle-like domain contrasts are observed in Ti_2Ni_3 precipitate. These contrasts were also observed in $Ti_2(Ni, Cu)_3$. The diffraction patterns of Ti_2Ni_3 precipitates which were obtained from 24 different orientations were observed, and those of $Ti_2(Ni, Cu)_3$ alloy were also observed. Typical electron diffraction patterns are shown in Fig. 2. Figures 2(a) and (b) are diffraction patterns of Ti_2Ni_3 precipitate, and (a′) and (b′) are

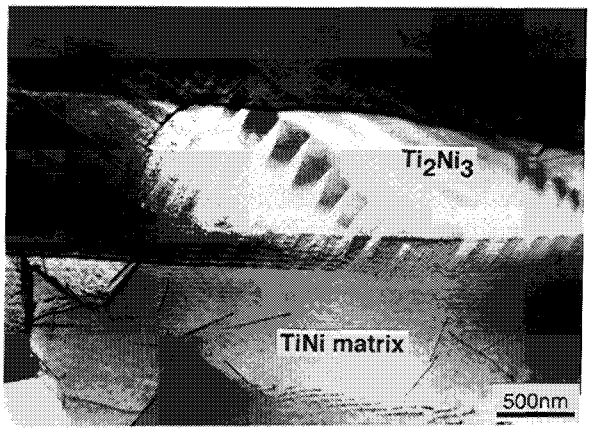

Fig. 1 Typical morphologies in Ti_2Ni_3 at room temperature. Twin related needle-like domains can be observed inside Ti_2Ni_3.

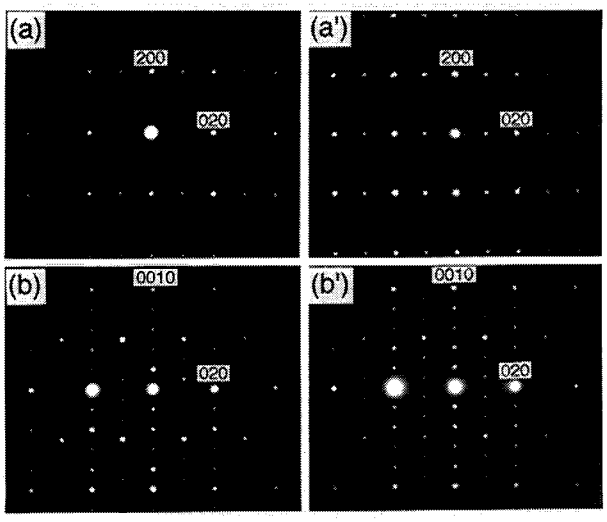

Fig. 2 Examples of the electron diffraction patterns of Ti_2Ni_3 precipitates ((a), (b)) and $Ti_2(Ni, Cu)_3$ alloy ((a'), (b')). Incident beams are parallel to $[001]_L$ for (a) and (a'), $[100]_L$ for (b) and (b'), respectively.

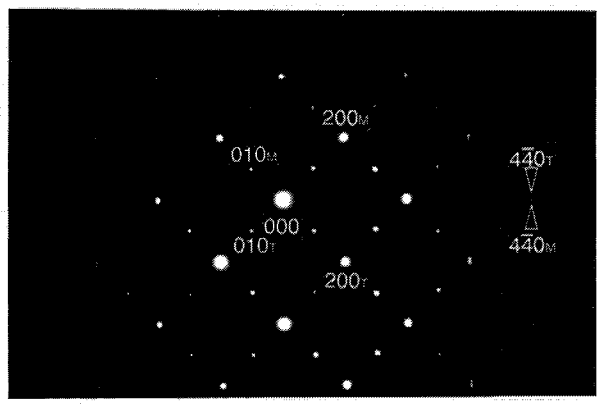

Fig. 3 Twinned diffraction pattern in Ti_2Ni_3 precipitates. Incident beam is parallel to $[001]_M$ and $[00\bar{1}]_T$. $4\bar{4}0_T$ and $4\bar{4}0_M$ spots split according to the small difference in the lattice parameters a and b. See text for details.

diffraction patterns of $Ti_2(Ni, Cu)_3$ alloy. Lattice parameters and the intensity distribution of the diffraction patterns in the $Ti_2(Ni, Cu)_3$ were also quite similar to those of Ti_2Ni_3 precipitates. In consequence, it is concluded that Ti_2Ni_3 and $Ti_2(Ni, Cu)_3$ have the same crystal structure consisting of 10 layers along the c-axis.

The lattice parameters of the low-temperature phase were reported by Nishida and Wayman[2]. They took the lattice parameters as $b=2a$. However, the twinning diffraction pattern shown in Fig. 3 indicates that $b\neq a$ nor $b\neq 2a$. If $b=a$ or $b=2a$, two spots indicated by arrows in Fig. 3 must be single spot. Careful analysis of the electron diffraction patterns were carried out, and the lattice parameters were determined to be $a=0.441$, $b=0.432$, $c=1.352$ nm and $\alpha=\beta=\gamma=90$ deg. The index of the twin boundary is $\{1\bar{1}0\}_L$ instead of $\{1\bar{2}0\}_L$ in this choice of the unit cell.

Nishida and Wayman[2] reported that the lattice of the low-temperature phase is monoclinic with $\gamma=89.3°$. The monoclinicity of this crystal will be mentioned in the next section. The precise lattice parameters is determined in the following X-ray diffraction.

Table 1 Obtained reflection conditions for the low-temperature phase of Ti_2Ni_3 precipitates. For $Ti_2(Ni, Cu)_3$ alloy, the same results were obtained.

hkl	$0kl$	$h0l$	$hk0$	$h00$	$0k0$	$00l$
$h+l$	k, l	$h+l$	h	h	k	l

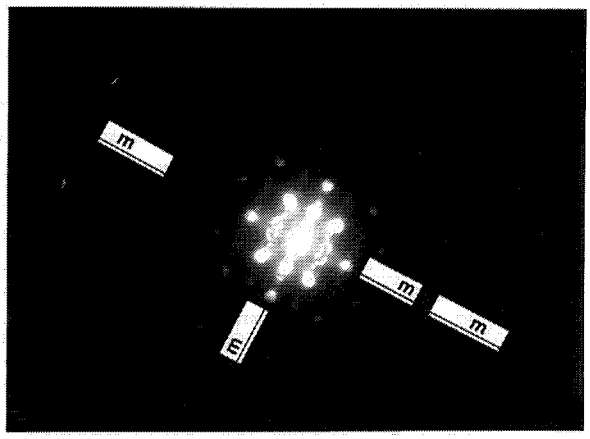

Fig. 4 An example of the CBED pattern in Ti_2Ni_3. Incident beam is parallel to $[1\bar{1}0]_L$. See text for details.

(1) Space group determination of the low-temperature phase

In order to determine the point group and the space group of the low-temperature phase, electron diffraction and CBED were observed. The diffraction patterns described above were used to find out the reflection conditions. Careful observations were made to avoid the wrong determination of the reflection conditions due to the double diffraction. For example, $0k0$ ($k=1, 3, 5$) reflections in Figs. 2(a) and (c) are those resulting from the double diffraction. Since the quality of this crystal was good, the reflection condition could be found easily as shown in Table 1. Comparison between this table and those of reflection conditions in the International Tables for Crystallography[7] shows that there is no possible space group in the monoclinic crystal system which satisfies the above conditions. The base centered orthorhombic system with the b-glide can satisfy these conditions. The orthorhombic crystal system with the above reflection conditions has four point groups, i.e. $mm2$, $m2m$, $2mm$ and mmm. The possible space groups in these point groups are $Bbm2$ (No. 40), $Bb2_1m$ (No. 36) and $Bbmm$ (No. 63).

A CBED pattern of Ti_2Ni_3 is shown in Fig. 4. This pattern was observed along the $[1\bar{1}0]_L$ direction. Symmetry elements in the whole pattern (W-P) of full and projection patterns are m and $2mm$, respectively. This leads to the projection diffraction group $2mm1_R$ and the diffraction group 2_Rmm_R. It is found that the point group that

satisfies these conditions is only *mmm* by using the table that shows the relationships among the point group, the diffraction group and the observed directions[8]. Among the above three possible space groups, the space group which belongs to the point group *mmm* is *Bbmm*. Therefore, the space group is determined to be *Bbmm* uniquely without using the consideration of the dynamical extinction rule. All CBED patterns taken along several directions agreed with this result consistently.

(2) High resolution electron microscopy observations

To refine the crystal structure with the least squares method, initial structure models are necessary. The initial structure models are required to satisfy the following conditions. (i) The structure consists of 10 layers stacking along the c-axis. (ii) The space group of the low-temperature phase is *Bbmm* that was obtained by the electron diffraction described above. The possible structure models satisfying the above conditions are only two and they are shown in Figs. 5(a) and (b). These two models have different stacking order along the c-axis. Structure models for the high-temperature phase were derived from these models. Crystal axes of the low- and the high-temperature phases are indicated in this figure. Van Loo *et al.*[3] and Nishida *et al.*[2] suggested that the structure of the high-temperature tetragonal phase of Ti_2Ni_3 is similar to that of Ti_2Cu_3 with the space group $P4/nmm$ (No. 129-2) determined by Schubert[9]. Both of the models in Fig. 5 belong to the space group $P4/nmm$. However, it should be noted that the stacking sequence along the c-axis of these two models are different from that of Ti_2Cu_3. The space group of the high-temperature phase will be discussed in Section III-2-(2).

HREM observations were carried out to determine which model is suitable. Figure 6(a) shows the example

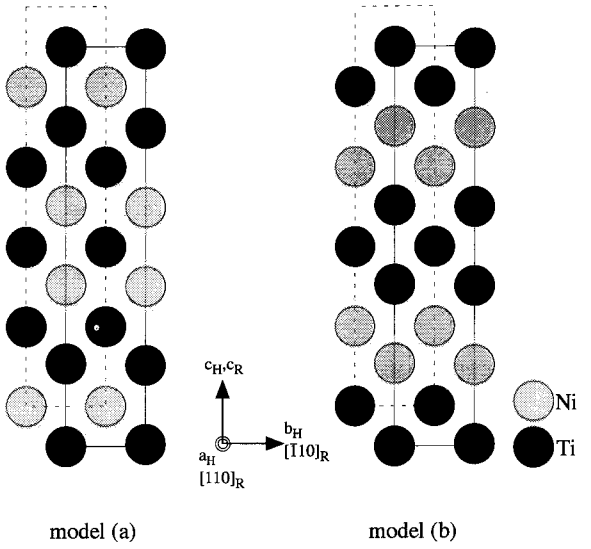

Fig. 5 Two possible structure models. Both models are based on the result of the electron diffraction experiments for the low-temperature phase. Atoms on the dotted lines are placed on the 1/2 upper plane of this figure plane.

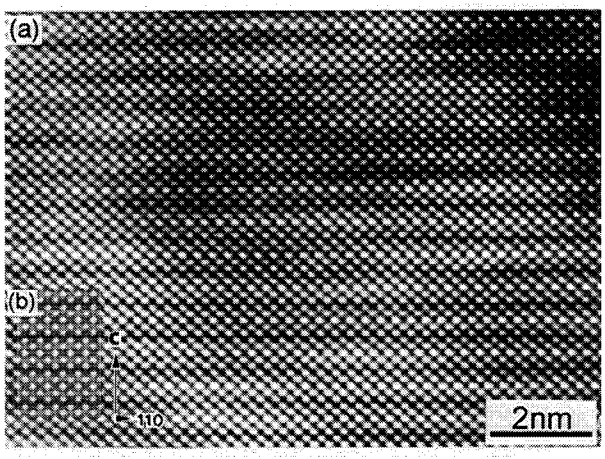

Fig. 6 (a) HREM observation taken along $[1\bar{1}0]_L$. (b) Result of the multislice calculation. The model (a) is assumed. This calculated image agrees well with the observed one.

of the observations. This photograph was taken along the $[1\bar{1}0]_L$ direction of the low-temperature phase. Figure 6(b) shows an result of the image simulation using the multislice calculation. In this image simulation, the crystal structure was assumed to be the model (a), the specimen thickness to be 11.0 nm and Δf to be -55.0 nm. The observed and calculated images agreed very well with each other. The characteristic dark contrast appearing at every five layers was reproduced in the simulation image. Thus the model (a) in Fig. 5 is more likely than the model (b). In addition, the model (a) is considered more stable than the model (b), that is, in the model (a), neighboring atoms of all the Ti atoms are Ni while in the model (b) are not. From these reasons, the model (a) was adopted as the initial structure model for the following Rietveld refinements.

2. X-ray diffractometer measurements

X-ray diffraction experiments were carried out to determine the precise lattice parameters and the crystal structure. The lattice parameters for Ti_2Cu_3[9] were used for indexing the diffraction pattern of the high-temperature phase, and all diffraction peaks could be indexed consistently.

(1) Lattice parameters determination

As mentioned in the previous section, the crystal structure of $Ti_2(Ni, Cu)_3$ is the same as that of the Ti_2Ni_3 precipitate. Since the split of the diffraction peaks can be observed clearly, $Ti_2(Ni, Cu)_3$ was used to observe the temperature dependence of the lattice parameters. Figure 7 shows the temperature dependence of the lattice parameters of $Ti_2(Ni, Cu)_3$ during heating. The transformation temperature was 333 K. The transformation temperature with cooling was 323 K, and the temperature hysteresis for the transformation was 10 K. The Pawley method was used to determine the precise lattice parameters and the initial values of the various fitting parameters for the following structure refinements. These calculations were carried out using the data meas-

Table 2 Lattice parameters and the final R-factors of the Pawley method calculations for $Ti_2(Ni, Cu)_3$ alloy.

Low temp. phase (298 K) Orthorhombic		High temp. phase (373 K) Tetragonal	
Lattice parameters	R-factors	Lattice parameters	R-factors
a=0.43806(1) nm	R_p=8.597%	a=0.30994(1) nm	R_p=8.542%
b=0.43405(3) nm	R_{wp}=11.346%	c=1.35826(5) nm	R_{wp}=11.467%
c=1.34472(3) nm	$R_{p(peak)}$=20.390%		$R_{p(peak)}$=20.932%

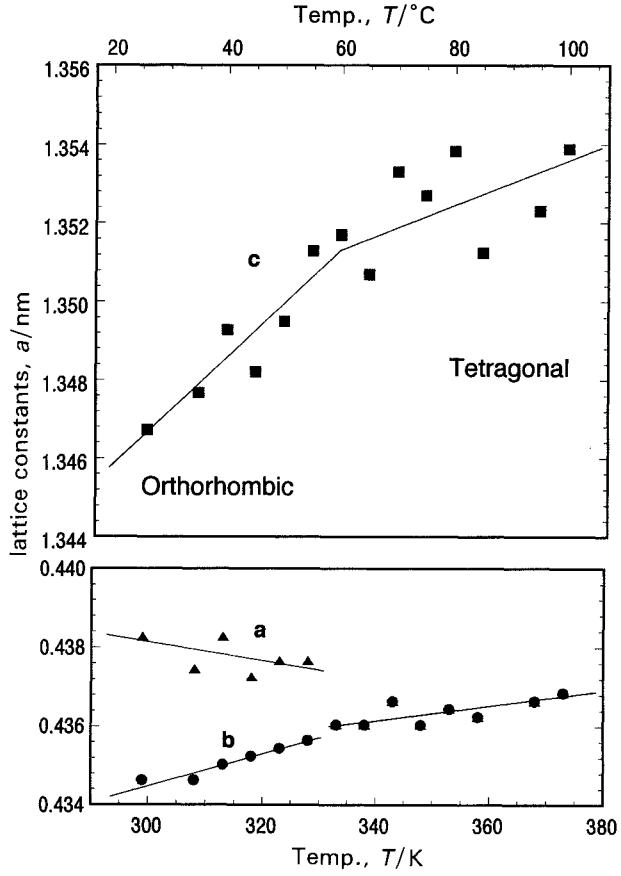

Fig. 7 Temperature dependence of the lattice parameters of $Ti_2(Ni, Cu)_3$ alloy on heating. Transformation temperature is about 330 K.

ured at 298 and 373 K for the low- and the high-temperature phases, respectively.

The lattice parameters and the final R-factors†† for $Ti_2(Ni, Cu)_3$ are shown in Table 2. The calculation results of the lattice parameters for Ti_2Ni_3 precipitates show almost the same values as those for $Ti_2(Ni, Cu)_3$. Details about Ti_2Ni_3 precipitates will be shown in Table 3 in the next section.

†† R-factors are defined as follows:

$$R_p=\frac{\Sigma|y_i(\mathrm{obs})-y_i(\mathrm{calc})|}{\Sigma y_i(\mathrm{obs})},\quad R_{wp}=\left\{\frac{\Sigma w_i(y_i(\mathrm{obs})-y_i(\mathrm{calc}))^2}{\Sigma w_i(y_i(\mathrm{obs}))^2}\right\}^{1/2}$$

$$R_{p(peak)}=\frac{\Sigma|y_i(\mathrm{obs})-y_i(\mathrm{calc})|}{\Sigma y_i(\mathrm{obs})^*},\quad y_i(\mathrm{obs})^*=y_i(\mathrm{obs})-b(\mathrm{calc})$$

$$R_I=\frac{\Sigma|I(\mathrm{obs})-I(\mathrm{calc})|}{\Sigma I(\mathrm{obs})},\quad R_F=\frac{\Sigma|\sqrt{I(\mathrm{obs})}-\sqrt{I(\mathrm{calc})}|}{\Sigma\sqrt{I(\mathrm{obs})}}.$$

The following lattice correspondence between the low- and the high-temperature phases are used in these indexing:

$$[100]_L /\!/ [1\bar{1}0]_H$$
$$[010]_L /\!/ [110]_H$$
$$[001]_L /\!/ [001]_H.$$

(2) Structure refinements

To determine the precise crystal structures of Ti_2Ni_3, the Rietveld refinements were carried out using both of the structure models described above. Atomic temperature factors B were fixed to be 0.8 throughout the refinements. As the result of the refinements, the model (a) in Fig. 5 showed lower R-factors than the model (b). This result is consistent with that of the HREM observations. Figure 8 is an example of the structure refinements. The full line and plus marks in the Fig. 8(a) represent the calculated curve and the observed diffraction pattern, respectively. The observed diffraction pattern in Fig. 8(a) obtained at room temperature shows that the specimen contains two phases, the TiNi matrix and the low-temperature phase of Ti_2Ni_3 precipitates. The model (a) is assumed for the precipitates in the calculated curve in Fig. 8(a). Figure 8(b) shows the calculated peak positions. The upper and lower sides of this figure are for the TiNi parent phase and the Ti_2Ni_3 precipitates, respectively. Figure 8(c) shows the difference between the observed and calculated diffraction patterns.

The space group $P4/nmm$ was assumed for the initial structure model for the high-temperature phase as described in the previous section. Judging from the final results of the refinements, however, atomic positions can be described with the space group $I4/mmm$ (No. 139) within their standard deviations. Therefore, the structure refinements were reexamined by assuming the space group $I4/mmm$ for models (a) and (b).

The obtained lattice parameters, atomic coordinates and the final R-factors for both the low- and the high-temperature phases are shown in Table 3(a) and (b), respectively. Interatomic distances for them are shown in Table 4. All values of the interatomic distances are considered to be proper values with considering the atomic radii of Ti and Ni atoms. Therefore, obtained crystal structure is considered as the proper one.

In these Rietveld refinements, other information can be obtained. For example, mass fractions for each phase and the composition of each phase are obtained. The fol-

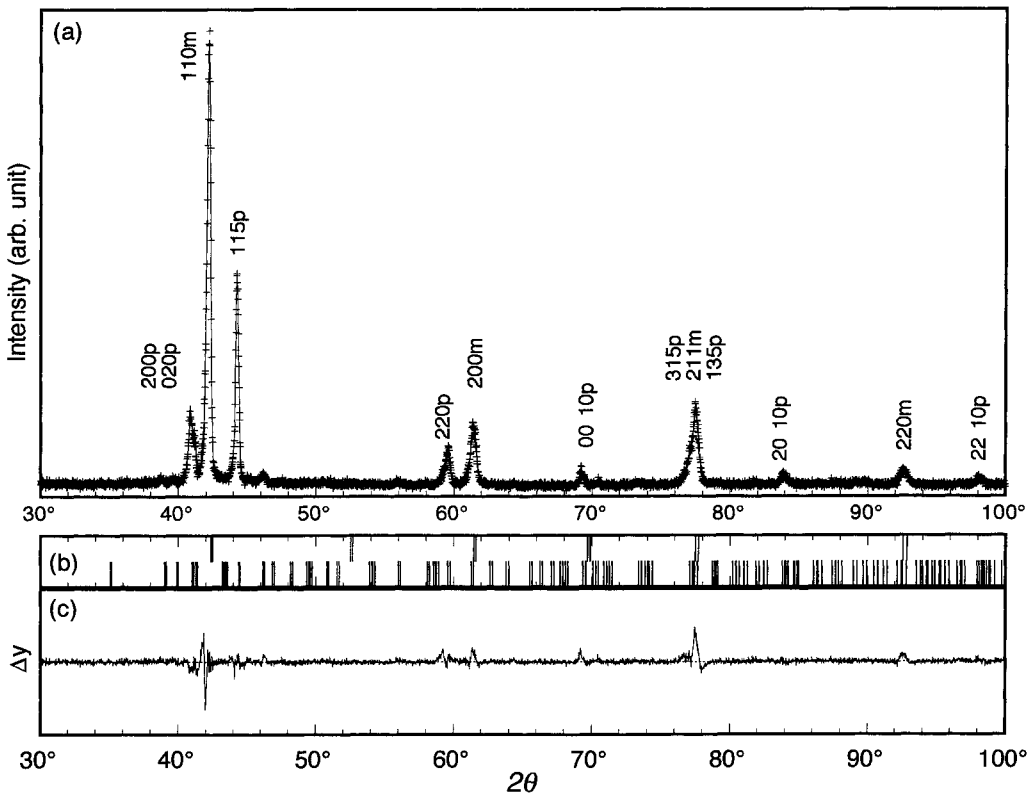

Fig. 8 An example of the calculation results of the Rietveld refinement. This figure represents that of the low-temperature phase of Ti_2Ni_3 precipitates and TiNi matrix . (a) Observed diffraction pattern (+ marks) and calculated pattern (full line). (b) Calculated peak positions. Upper and lower side mean the peak positions for TiNi matrix and Ti_2Ni_3 precipitates, respectively. (c) The deviation between observed and calculated intensities.

Table 3 Results of the Rietveld refinements for Ti_2Ni_3 precipitates. See text for details.

	(a) Low temp. phase (298 K)				(b) High temp. phase (373 K)			
Crystal system Space group	Orthorhombic *Bbmm*(#63)				Tetragonal *I*4/*mmm*(#139)			
Pearson symbol, Structure type	*oC*20		Pd_3Ti_2 type		*tI*10		Al_3Os_2 type	
Lattice parameters (nm)	a=0.4398(49)	b=0.4370(48)	c=1.3544(150)		a=0.3095(38)	c=1.3585(169)		
Atomic coordinates		x	y	z		x	y	z
	Ti1(8g)	0.227(57)	1/4	0.106(4)	Ti(4e)	0	0	0.391(4)
	Ni1(4c)	0.725(74)	1/4	0	Ni1(4e)	0	0	0.196(4)
	Ni2(8g)	0.232(37)	1/4	0.300(5)	Ni2(2a)	0	0	0
R-factors	R_{wp}: 14.11%		R_p: 10.64%		R_{wp}: 14.55%		R_p: 11.03%	
Ti_2Ni_3 Precipitates	R_I: 8.24%		R_F: 8.53%		R_I: 6.72%		R_F: 5.65%	
Matrix (parent phase)	R_I: 7.41%		R_F: 5.52%		R_I: 4.41%		R_F: 3.37	

lowing calculation results were obtained in the refinements: (i) Mass fraction of matrix and precipitates was 78 and 22%, respectively. (ii) The composition of the matrix after aging was calculated as 49.85 at.%Ti-50.15 at.% Ni. Ni contents in the matrix were reduced from 52 at.% after Ti_2Ni_3 had been precipitated. All these calculated values are considered as the appropriate values in comparison with other observations by optical and electron microscopy. These support that the calculation processes are correct.

The structural study in this paper reveals the characteristic of the Ti_2Ni_3 transformation. The volume changes discontinuously at the transformation temperature, as shown in Fig. 7. The hysteresis was also observed in the measurements of the lattice parameters. The crystal structure of the low-temperature phase is obtained from the high-temperature phase without diffusion. These feature suggest the conclusion that the transformation of Ti_2Ni_3

Table 4 Interatomic distances in Ti_2Ni_3 precipitates. (a) Low temperature phase. (b) High temperature phase.

(a) Low temperature phase			(b) High temperature phase		
Atom(1)	Atom(2)	Distance(/nm)(std.)	Atom(1)	Atom(2)	Distance(/nm)(std.)
Ni(1)	Ti×2	0.253(2)	Ti	Ni(1)×4	0.249(4)
	Ti	0.253(2)		Ni(2)×4	0.264(4)
	Ti	0.254(2)		Ni(1)×2	0.264(9)
	Ni(1)×2	0.257(2)	Ni(1)	Ti×4	0.249(4)
	Ni(1)×2	0.258(2)		Ni(1)×4	0.263(7)
Ni(2)	Ti	0.261(3)		Ti	0.264(9)
	Ti×2	0.263(2)		Ni(1)	0.267(7)
	Ti×2	0.263(2)	Ni(2)	Ti×8	0.264(4)
	Ti×2	0.263(2)		Ni(1)×2	0.267(7)
	Ti×2	0.264(2)			
	Ni(1)×2	0.271(3)			
Ti	Ni(1)×2	0.253(2)			
	Ni(1)	0.253(2)			
	Ni(1)	0.254(2)			
	Ni(1)	0.261(3)			
	Ni(2)	0.263(2)			
	Ni(2)×2	0.263(2)			
	Ni(2)	0.264(2)			

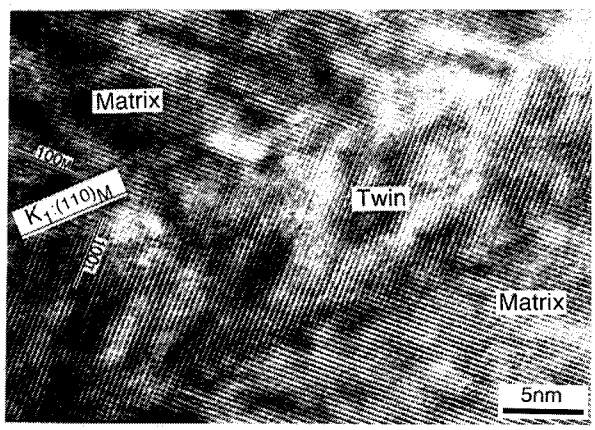

Fig. 9 HREM observation of the twin in the low-temperature phase in Ti_2Ni_3 precipitates. See text for details.

is the first-order martensitic transformation. The transformation mechanism of Ti_2Ni_3 was discussed by Nishida and Wayman[10]. They assumed that the transformation is martensitic, and pointed out that the similarity to the R-phase transformation in Ti-Ni. However, the crystal structure obtained above is quite different from that of the R-phase[11]. Therefore, at present, it is hard to consider that the transformation mechanism of Ti_2Ni_3 is the same as that of R-phase transformation.

3. Twinning in the low-temperature phase

The low-temperature phase has internal twins, whose twin plane was $\{110\}_L$ as shown in Section III-1. The twin boundaries in Fig. 1 are not straight, and the twinning mode is the compound type. HREM observations were carried out to obtain the information on this twin boundary structure. Figure 9 shows the lattice image around the twin boundary in Ti_2Ni_3 precipitates. The twin boundaries are not sharp in this observation.

Table 5 Calculated twinning elements for the low-temperature phase. Lattice constants used for this calculation are those obtained for Ti_2Ni_3 precipitates.

η_1	K_1	η_2	K_2	s
$\langle\bar{1}10\rangle$	$\{110\}$	$\langle110\rangle$	$\{\bar{1}10\}$	0.013

HREM observation showed that there was a transition region from matrix to twin around the boundary, and the lattice fringes of the matrix and twin crystal overlap in this region. Twin boundaries of the compound twins in other martensite phase, such as γ_1' Cu-Al-Ni and γ_2' Au-Cd[12], show the similar feature. In general, the boundaries of the compound twin were observed not to be sharp plane. The boundary structure of these compound twins may be understood by considering the magnitude of the twinning shear. Table 5 shows the twinning elements calculated by the Bilby-Crocker theory[13] with the obtained lattice parameters of Ti_2Ni_3. The extremely small twinning shear is probably the origin for the curved twin boundaries pointed out in the above.

IV. Conclusions

The Ti_2Ni_3 precipitate in Ti-Ni alloy system transform martensitically near the ambient temperature. The crystal structure of both high- and low-temperature phases, and twinning in the low-temperature phase were studied in detail, by critical experiments and analyses employing various techniques such as TEM, electron diffraction, CBED and the powder X-ray diffraction with the Pawley and Rietveld analyses. As a result the following conclusions were obtained.

(1) The crystal structure of the high-temperature phase is tetragonal with Pd_3Ti_2 type. The space group was found to be $I4/mmm$, and the atomic parameters

were determined accurately by the least squares method. The lattice parameters determined by the Rietveld method were: $a=0.3095(38)$ and $c=1.3585(169)$ nm.

(2) The crystal structure of the low-temperature phase is orthorhombic with Al_3Os_2 type. The space group was found to be *Bbmm*, and the atomic parameters were accurately determined. The lattice parameters determined were: $a=0.4398(49)$, $b=0.4370(48)$ and $c=1.3544(150)$ nm.

(3) The twins in the low-temperature phase were found to be {110} compound twins, whose twinning elements were calculated by the Bilby-Crocker theory, and the characteristic of the twin boundary was studied by high resolution electron microscopy.

Acknowledgments

The authors are grateful to Dr. K. Ishii for allowing us to use TEM, and Dr. Y. Bando, for the multislice program. They also wish to thank Messrs. J. Kazama and S. Kato for their assistance on the part of the experiments in this paper.

REFERENCES

(1) M. Nishida, C. M. Wayman and T. Honma: Met. Trans., **17A** (1986), 1505.
(2) M. Nishida and C. M. Wayman: Met. Trans., **18A** (1987), 785.
(3) F. J. J. Van Loo, G. F. Bastin and A. J. H. Leenen: J. Less-Common Met., **57** (1978), 111.
(4) M. Nishida, T. Ueda, Y. Toyama and A. Chiba: Mater. Sci. Forum, **56-58** (1990), 599.
(5) H. Toraya: *The Rietveld method. chapt. 14*, Ed. by R. A. Young, Oxford, (1993), p. 254.
(6) F. Izumi: *The Rietveld method. chapt. 13*, Ed. by R. A. Young, Oxford, (1993), p. 236.
(7) *International Tables for Crystallography*, 2nd edition, Vol. A, Kluwer Academic Publishers, (1989).
(8) B. F. Buxton, J. A. Eades, J. W. Steeds and G. M. Rackham: Phil. Trans., **281** (1976), 171.
(9) K. Schubert: Z. Metallkde, **56** (1965), 197.
(10) M. Nishida and C. M. Wayman: *Proc. Int'l. Conf. on Martensitic Transformations '86*, Japan Inst. Metals, (1986), p. 653.
(11) T. Hara, T. Ohba and K. Otsuka: J. de Phys. IV, **C8** (1995), 641.
(12) T. Hara, T. Ohba, K. Otsuka, Y. Bando and S. Nenno: *Proc. Int'l. Conf. on Martensitic Transformations '92*, Monterey Institute of Advanced Studies, (1993), p. 257.
(13) B. A. Bilby and A. G. Crocker: Proc. Roy. Soc. Ser. A, **288** (1965), 240.